Peer-reviewed version available at Atmosphere 2019, 10, 36; doi:10.3390/atmos10010036

Article

Summertime Urban Mixing Layer Height over Sofia, Bulgaria

Ventsislav Danchovski [1]

[1] Department of Meteorology and Geophysics,Faculty of Physiscs, Sofia University, Sofia, 1164, Bulgaria; danchovski@phys.uni-sofia.bg

Version November 8, 2018 submitted to Preprints

Abstract: Mixing layer height (MLH) is a crucial parameter for air quality modelling that is still not routinely measured. Common methods for MLH determination use atmospheric profiles recorded by radiosonde but they suffer from course temporal resolution since balloon launching is only twice a day. Recently cheap ceilometers are gaining popularity in the retrieval of MLH diurnal evolution based on aerosol profiles. This study presents a comparison of a proprietary (Jenoptik) and a free available (STRAT) algorithms to retrieve MLH diurnal cycle. The comparison is accomplished in summer season over urban area and radiosonde data is used to estimate MLHs according to parcel, lapse rate, and Richardson methods (the last algorithm is used as a reference in the study) in addition. It was found that STRAT and Jenoptik give lower MLH than radiosonde with an underestimation of about 150m and 650m respectively. Additionally, STRAT showed reasonable performance in tracking of MLH diurnal evolution. Daily MLH maximum of about 2000m was found in the late afternoon (18-19 LT). In contrast, Jenoptik algorithm showed more weaknesses, mainly attributed to its real-time operation and independent processing of a single profile. At night and during morning transition period, both lidar-based methods showed difficulties as MLH was often in the ceilometer's incomplete overlapping zone so residual or advected aerosol layers aloft were misleadingly reported as mixing layer (ML).

Keywords: mixing layer, urban area, ceilometer, radiosonde

PACS: 01.30.-y, 01.30.Ww, 01.30.Xx

1. Introduction

Air quality impact on human health is an actual problem especially in densely populated areas. Hence, a lot of effort are being made to better understand the processes controlling pollution levels, especially in numerical modelling. Key input parameters of these models are meteorological variables, as they are needed to be known in calculating of production, diffusion, transport and scavenging of atmospheric pollutants. These harmful substances are dispersed vertically within the ML due to its inherent turbulence. According to Seibert et al. [1], ML is "... the layer adjacent to the ground over which pollutants or any constituents emitted within this layer or entrained into it become vertically dispersed by convection or mechanical turbulence within a time scale of about an hour". Obviously, near ground pollution levels will depend on the MLH since it constrains the dispersion volume, so the MLH is crucially important to be known especially at urban areas where pollution sources and inhabitants are much more [2–9]. Moreover, urban MLH can be characterized by enormous temporal and spatial variability due to inhomogeneity in surface roughness and heating in the cities. Therefore it is worth to be continuously monitored and also compared with parametrizations in numerical weather and/or pollution prediction models [10–12].

Despite its importance, MLH is not a part of routine measurements. Besides, as it is associated with spatial distribution of the turbulence we need "a turbulence profiler" to determine it. Doppler lidars [13] and sodars [14,15] might serve as such profilers but the first are quite expensive and the second have limited vertical range. However, vertical profiles of non-reactive scalar meteorological

variables should be nearly constant with height within well mixed boundary layer [16] so we might detect the MLH by looking for abrupt change in uniformly distributed profiles of these tracers [17,18].

Regardless of the wide variety of remote sensing methods, the most utilized instrument for MLH detection is the radiosonde and it is still used as a reference. The deriving of the MLH from temperature, humidity and wind profiles recorded during the radiosonde flight dates back to 1960s [19], but these radiosonde-based methods are still used individually [20] or for validating the retrieved by different remote sensing instruments MLHs [21]. However, the radiosonde also has some drawbacks as it measures atmospheric properties along its flight, which is not vertical, but slant due to horizontal wind. Therefore, the radiosonde profiles do not coincide with rising thermals or vertical profiles derived from the remote sensing instruments. Additionally, the radiosondes main limitation is their coarse temporal resolution since they are usually launched not more than twice a day.

The necessity of MLH continuous monitoring can be met by operating of ground based remote sensing instruments. A comprehensive review of existing techniques for MLH determination through ground-based remote sensing instruments with their advantages and limitations can be found in Wiegner et al. and Emeis et al. [22,23]. It is worth to remark that individual disadvantages of each instrument in MLH diurnal cycle determination can be overcome if apparatuses are used in combination [24]. In the last years laser-based remote sensing instruments, especially ceilometers become more affordable and widely used in the field of atmospheric research in particular in MLH determination [25–32]. Different lidar-based methods for retrieving of the MLH from range corrected signal are summarized in Haeffelin et al. [33]. These methods are the basis of many proprietary [34,35] and in-house [36–39] algorithms explicitly designed for MLH retrieving from ceilometer's data. Possible performance improvement of these lidar-based techniques might be achieved by monitoring of diurnal variations in Radon-222 [40] or it can be used for MLH evaluation individually [41].

The objectives of the present study are to evaluate ceilometer's MLH detection performance in urban area by comparison of a proprietary and a popular free available algorithm. Both methods are assessed against retrieved MLHs from radiosonde profiles as a reference. Structure and evolution of the mixing layer over Sofia in summer are also discussed.

The paper is organized as follow: details about the data and methods are in section 2; results and discussions are in section 3; article ends with summary of findings.

2. Data and Methodology

Sofia is the largest and the most densely populated city in Bulgaria. The city is located in a valley that is almost fully encircled by mountains so the micro- and meso-scale processes as well as the ML dynamics are heavily influenced by both complex orography and urban territory. To perform our analysis of urban MLH we used 3 month of intensive measurements, from June 1 until August 31, 2015. The data used in this study are obtained from a continuously operating ceilometer Jenoptik CHM 15k, and a balloon sounding launched on a daily basis at 12:00 UTC (14:00 LT).

The CHM15k is operated by the Department of Meteorology and Geophysics, Sofia University. The ceilometer is situated in the city centre on the territory of the University Astronomical Observatory in park "Borisova gradina" (Figure 1). The CHM15k is an eye-safe biaxial lidar system equipped with Nd :YAG solid-state near-infrared laser operating at 1064nm. It emits pulses with energy 8μJ and repetition frequency 5-7kHz. Measuring range of the ceilometer is 30-15000m with 15m resolution, temporal resolution is set to 60s, further details about the instrument can be found in [42].

The MLH is retrieved from ceilometer profiles by supposing that aerosol concentration is rapidly adapted to thermal stratification of the ML and aerosol loading above the city is not dominated by advection. Manufacturer's software includes proprietary algorithms for automatically deriving of the MLH every minute (software version 1.56) [43]. A free available Structure of the Atmosphere (STRAT) algorithm [37] which is designed for retrieving of aerosols vertical profiles in atmospheric boundary layer and free troposphere is used for comparison. In contrast to the Jenoptik algorithm that is based

on vertical gradient of backscatter signal in a single profile, STRAT utilizes both horizontal and vertical gradients by using Sobel 2-D derivation operators [33].

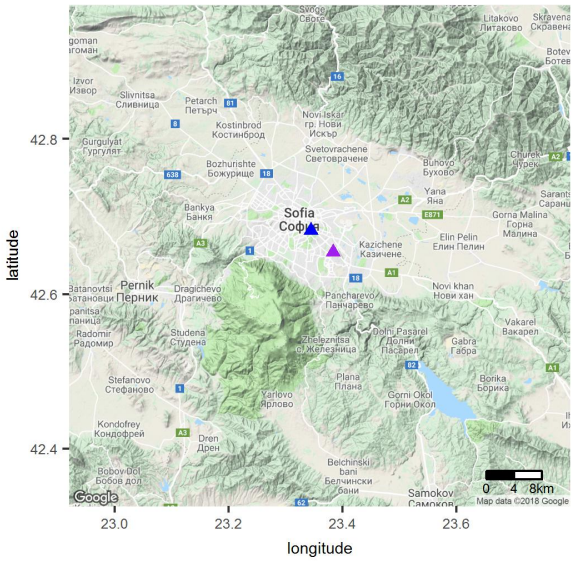

Figure 1. The locations of the ceilometer and the radiosonde indicated by a blue and a purple triangles in the Sofia valley.

The atmospheric sounding system is Vaisala's MW41 that is located in the Central Aerological Observatory on the territory of the National Institute of Meteorology and Hydrology, which is about 4.4 km south-east from the ceilometer (Figure 1). In this study low resolution radiosonde data are used, free available at Integrated Global Radiosonde Archive (IGRA) [44]. Archived radiosonde data are consisted of atmospheric parameters recorded at mandatory and significant levels which were used to restore the atmospheric profiles by linear interpolation.

Following de Haij et al. [45] three different MLH detecting algorithms are applied to the radiosonde data. Bulk Richardson (Ri) method is based on the Richardson number which is the ratio of thermally and mechanically driven turbulence. According to the method MLH is the level where the bulk Richardson number exceed predefined threshold value [46–48]. Here commonly recommended value of 0.21 is used. It is also worth to note that the Ri method is suitable for both convective and stable conditions. In contrast, the parcel method [19,49] provides reliable results only for unstable convective boundary layer since method neglects wind shear effects on vertical mixing. MLH in this method is determined by extending dry adiabatically surface temperature to its intersection point with temperature profile. The last method for MLH determination from radiosonde data is the lapse rate method [50]. It is based on threshold values of vertical gradients of potential temperature (θ) and relative humidity (RH), adhering to de Haij et al. [45] negative gradient of RH and gradient of θ >2K/km are used as basis in this work. As the selected critical value of potential temperature gradient is more or less subjectively chosen, performance of lapse rate values 0.5, 1, 1.5, 2.5, 3, 3.5, and 4K/km is also tested.

As main synoptic-scale systems are associated with suppressing or stimulating of parcel ascending it is interesting to verify their role to mixing layer height [51]. Therefore, the difference of surface layer atmospheric pressure (atm.press) and its smoothed value (obtained by low pass filter with cutoff 6 days) is standardized and atmospheric pressure is classified as "Low" if the standardized difference is smaller than 0.5, "High" for higher than 0.5 and if the standardized values are in between atmospheric pressure is marked as "Normal".

Preprints (www.preprints.org) | NOT PEER-REVIEWED | Posted: 8 November 2018 doi:10.20944/preprints201811.0187.v1

Peer-reviewed version available at Atmosphere 2019, 10, 36; doi:10.3390/atmos10010036

3. Results and Discussions

3.1. Intercomparison of Radiosonde-based MLH Retrieving Methods

The three aforementioned radiosonde-based algorithms for MLH estimation are firstly compared against one another on Figure 2. The perfect correlation between Richardson and parcel methods indicates that in summer at 14:00 LT (12:00 UTC) urban mixing layer in Sofia is dominated by thermally driven turbulence. It is a fairly expected result since the studied period is summer and radiosonde launching is in early afternoon. It is also evident that higher MLH values are related to prevailing low atmospheric pressure, but if atmospheric pressure is marked as normal or high MLHs are on average lower.

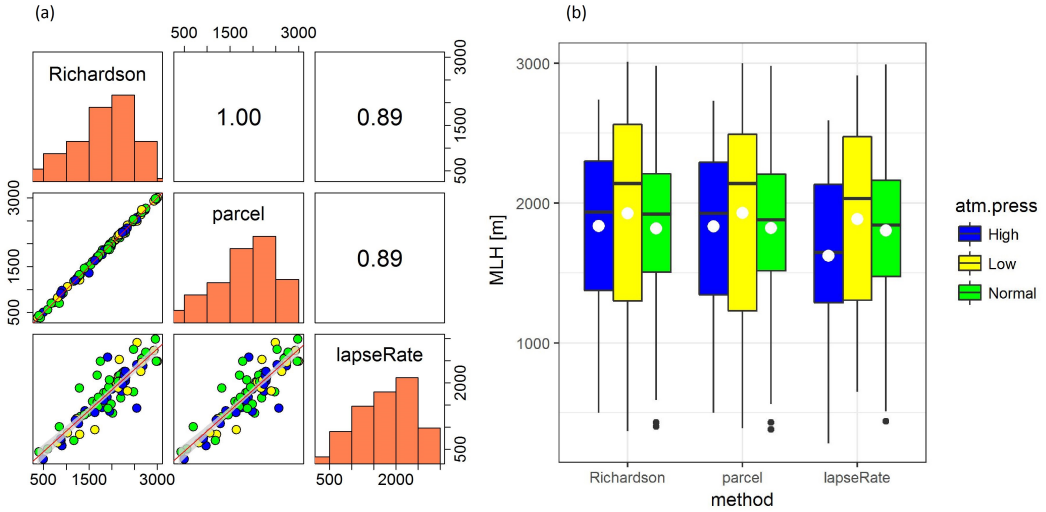

Figure 2. Intercomparison of the three radiosonde-based MLH methods. The correlation matrix (**a**) shows correlation coefficients in upper-right triangle, the diagonal shows histogram of each method, lower-left triangle is filled with scatterplots and linear regression lines with corresponding 95% confidence intervals. The box and whiskers plot (in the style of Tukey) is on the plot (**b**). The boxes hinges correspond to the 25, 50 and 75 percentiles. The lower and upper whiskers represent the lowest values still within 1.5 IQR (inter-quantile range) of the lower quartile, and the highest values still within 1.5 IQR of the upper quartile Data beyond the end of the whiskers are marked as outliers and plotted as black dots. White dots indicate mean values. In both figures, atmospheric pressure is color-coded as "High" - blue, "Low" — yellow, "Normal" - green

Obviously, lapse rate method shows a worse agreement with Richardson and parcel ones, especially if atmospheric pressure is high. Therefore, it is tested how threshold value of vertical gradient of θ influences concurrence with other two approaches. It is found that lapse rate values 1, 1.5 and 2K/km perform similarly and Pearson correlation coefficients with respect to Ri method are about 0.89. However, correlation diminishes if smaller or higher threshold values are preferred. It is also worth to mention that negative vertical gradient of relative humidity is not varied as it agrees with mixing layer conception since earth's surface is water vapour source and free atmosphere is low in humidity. Based on Richardson and parcel methods consistency and taking into account that the first one incorporates both mechanical and bouncy production of turbulent mixing Ri method is used as a reference in the following analysis. Performance of parcel and lapse rate method based on above mention set of critical values against Richardson method is evaluated and summarised in Table 1.

Preprints (www.preprints.org) | NOT PEER-REVIEWED | Posted: 8 November 2018 doi:10.20944/preprints201811.0187.v1

Peer-reviewed version available at Atmosphere 2019, 10, 36; doi:10.3390/atmos10010036

Table 1. Skill scores (MD – mean deviation; RMSD – root-mean-square deviation, r – Pearson correlation coefficient, slope –linear regression slope, intercept – linear regression intercept) of parcel and lapse rate methods against Richardson as a reference in MLH determination

method	MD	RMSD	r	slope	intercept
parcel	1	37	1.00	0.99	11
lapse rate 0.5K/km	-215	396	0.85	0.82	520
lapse rate 1.0K/km	-200	351	0.89	0.88	402
lapse rate 1.5K/km	-194	342	0.89	0.89	388
lapse rate 2.0K/km	-153	330	0.89	0.85	417
lapse rate 2.5K/km	-87	403	0.81	0.75	554
lapse rate 3.0K/km	-40	431	0.78	0.70	601
lapse rate 3.5K/km	39	493	0.75	0.61	719
lapse rate 4.0K/km	106	543	0.73	0.57	773

3.2. Intercomparison of MLHs Derived from Ceilometer and Radiosonde data

MLHs retrieved from radiosonde data are often treated as referent since they are based on thermodynamic structure of lowest atmosphere that directly reflects changes in surface forcing. However routine balloon launching is only twice a day so it does not allow MLH diurnal evolution to be tracked. Cheap ceilometers that provide backscatter power profiles are tempting alternative as they operate continuously.

In order to evaluate overall performance of ceilometer-based methods in MLH determination the retrieved values are compared against estimated by Richardson method from radiosonde data. As the radiosonde is launched once a day at 12:00 UTC (14:00 LT), retrieved from ceilometer MLHs within timespan of 20 minutes are averaged and used in the comparison. The left and right panels of Figure 3 show a correlation matrix and box and whiskers plots of MLHs determined by STRAT, Jenoptik and Ri methods at different atmospheric pressure. It is evident that both ceilometer based algorithms tend to underestimate MLH compered to radiosonde (Richardson). Surprisingly, the already established tendency the radiosonde to report higher MLH at low pressure is not observed in ceilometer-derived values. This might be a result of the ceilometer's difficulties in detecting MLH in cloudy and rainy weather, which can occur at low atmospheric pressure systems.

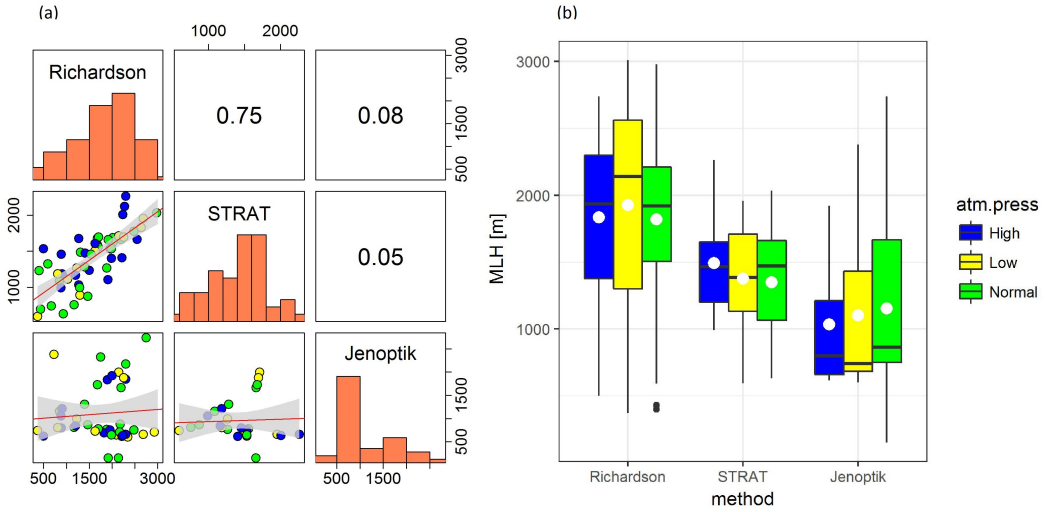

Figure 3. A correlation matrix (**a**) and Tukey's box and whiskers plot (**b**) of radiosonde- (Richardson) and lidar-based (STRAT and Jenoptik) algorithms for MLH detection. Conventions are the same as in Figure 2.

Skill scores of lidar-based algorithms against Ri method are listed in Table 2. It can be seen that average underestimation of MLH by STRAT and Jenoptik is 150m and 650m respectively. Obviously

Preprints (www.preprints.org) | NOT PEER-REVIEWED | Posted: 8 November 2018 doi:10.20944/preprints201811.0187.v1

Peer-reviewed version available at Atmosphere 2019, 10, 36; doi:10.3390/atmos10010036

estimated by STRAT values of MLH are reasonably comparable with those retrieved from radiosonde profiles but Jenoptik's performance is quite unpromising and needs further clarification.

Table 2. Skill scores (MD – mean deviation; RMSD – root-mean-square deviation, r – Pearson correlation coefficient, slope –linear regression slope, intercept – linear regression intercept) of aerosol-based algorithms (Jenoptik and STRAT) against Richardson method as a reference in MLH determination

method	MD	RMSD	r	slope	intercept
Jenoptik	-665	1086	0.08	0.0.7	970
STRAT	-162	467	0.75	0.45	701

3.3. Diurnal Evolution of MLH Determined by Ceilometer – A Case Study

In order to elucidate abovementioned ceilometer's capacity to track the MLH diurnal cycle a case study is first considered. In Figure 4 diurnal evolution of range-corrected ceilometer signal on July 24 is presented along with MLH determined according to STRAT and Jenoptik algorithms, radiosonde derived MLH by Richardson method is also plotted for comparison.

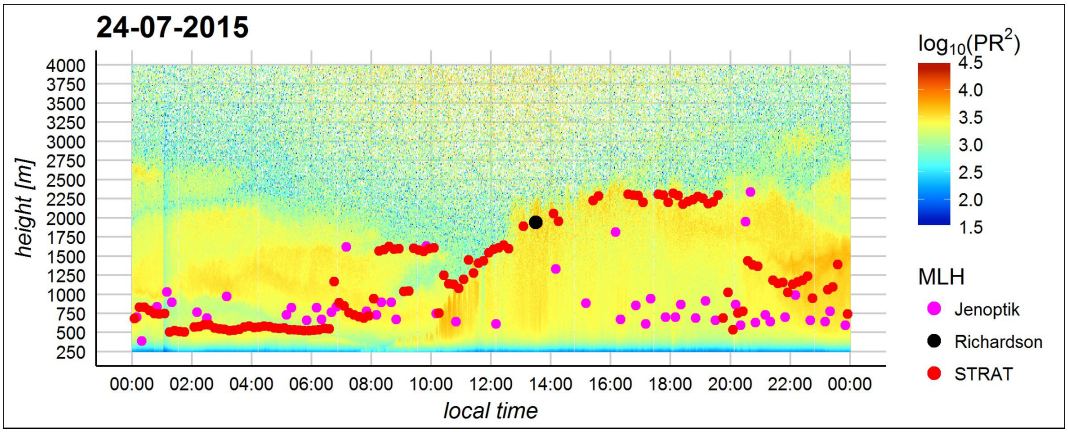

Figure 4. Time-height cross section of range-corrected ceilometer backscatter power(in arbitrary units) on 24 July 2015. The MLH retrieved from ceilometer's data by Jenoptik and STRAT algorithms are marked by magenta and red dots, respectively. Radiosonde-based MLH according to Ri method is presented by a black dot.

Obviously, range corrected ceilometer's signal reveals some characteristic features in MLH diurnal evolution. Backscatter signal within first 500-700m is high in the wee hours of the night that might be associated with mechanically mixed aerosols within nocturnal boundary layer. Above that layer, there is a zone with decreased signal that is capped by a high backscatter layer, which most likely outlines aerosol burden air in residual layer, or it is a result of advection at that elevation. Ceilometer's signal also depicts daytime evolution of MLH with its typical growing due to solar heating of the surface. After sunrise thermals start forming and rising as result of positive buoyancy. These updrafts produce turbulent mixing so the diminished vertical backscatter within ML in the afternoon is due to increased volume for aerosol dispersion. Enhanced signal close to ML top in the afternoon might be attributed to hygroscopic grow of aerosols due to increased relative humidity. Obviously, MLH reach its maximum ($\sim$2250m) at $\sim$16:00 LT and it is almost constant until $\sim$19:00 LT. In the evening solar elevation angle starts decreasing and sun sets, resulting in cutting of energy source for thermally driven turbulence, new nocturnal layer starts forming and air aloft associated with new residual layer becomes decoupled from mechanical source of turbulence on the ground. As can be seen MLH determined by Ri method is $\sim$1940m that corresponds certainly well on aerosol distribution depicted by ceilometer backscatter signal at the moment of balloon launching (at 13:30 LT that day).

It is also noticeable that STRAT algorithm represents diurnal evolution of MLH plausibly. However, in the time interval from sunrise (6:09 LT) to approximately 10:30 LT which correspond to morning transition period STRAT misleadingly reports a backscatters gradient aloft (associated with residual layer) as a MLH instead of closest to the ground one. Similar behaviour is found in all days and it seems to be a result of layer attribution technique implemented in STRAT. According to Haeffelin et al. [33] the algorithm reports the strongest, the second strongest and the lowest gradients in backscatter then depending on local time it constructs diurnal evolution of its "best estimate" (used here as MLH) as the lowest gradient at night and the strongest during the day. Thus, the STRAT reports abrupt changes in MLH around sunrise and sunset instead of smooth transition from nocturnal to convective boundary layer and vice versa. Possible improvement of layers attribution and representation of MLH diurnal evolution can be achieved by incorporation of some statistical analysis [52] or graph theory [53].

It can be seen that consistency of MLHs reported by Jenoptik algorithm with observed aerosol vertical distribution and temporal evolution is worse than STRAT. The performance of Jenoptik method during the daytime is much poorer and it hardly represents MLH evolution. Obviously, Jenoptik significantly underestimates ML heights in early afternoon when MLH is much higher and still growing. That worse performance of Jenoptik method is supposed to be a result of algorithm operation because it provides real-time information about MLH retrieved from single profile in contrast to STRAT that exploits daylong data.

Evidently, both ceilometer-based methods have trouble with backscatter gradient detection and layer attribution from ∼13:00 LT to ∼15:00 LT when reported MLHs are only few. That period is characterized by reduced backscatter since aerosol concentration is diminished due to ML growing in combination with high solar elevation angle. These factors can result in reduced signal to noise ratio (due to enhanced background radiation and decreased backscatter signal) and thus MLH becomes more difficult to be detected.

3.4. Diurnal Evolution of MLH Determined by Ceilometer – A Statisitcal Analysis

The aforementioned features of both lidar-based techniques are also visible if all data for MLH daytime progress are summarised and presented as a boxplot (Figure 5).

Evidently, STRAT outperforms Jenoptik in tracking of expected MLH diurnal evolution. An average MLH at night in summer is surprisingly high - about 1000m. As was already underlined, at night MLH detection by ceilometer is tough due to difficulties with layer attribution and frequent reporting of the residual layer aloft as MLH, therefore true values should be much lower. The daily maximum of MLH (often more than 2000m) is registered in the late afternoon (∼18:00 LT), few hours before sunset and more importantly during most intensive car traffic, which can help against excessive concentrations of air pollution. It is worth noting large number of outliers in the retrieved MLHs by Jenoptik algorithm, most of them are related to high aerosol layers due to advection or residual layers at night.

Preprints (www.preprints.org) | NOT PEER-REVIEWED | Posted: 8 November 2018 doi:10.20944/preprints201811.0187.v1

Peer-reviewed version available at Atmosphere 2019, 10, 36; doi:10.3390/atmos10010036

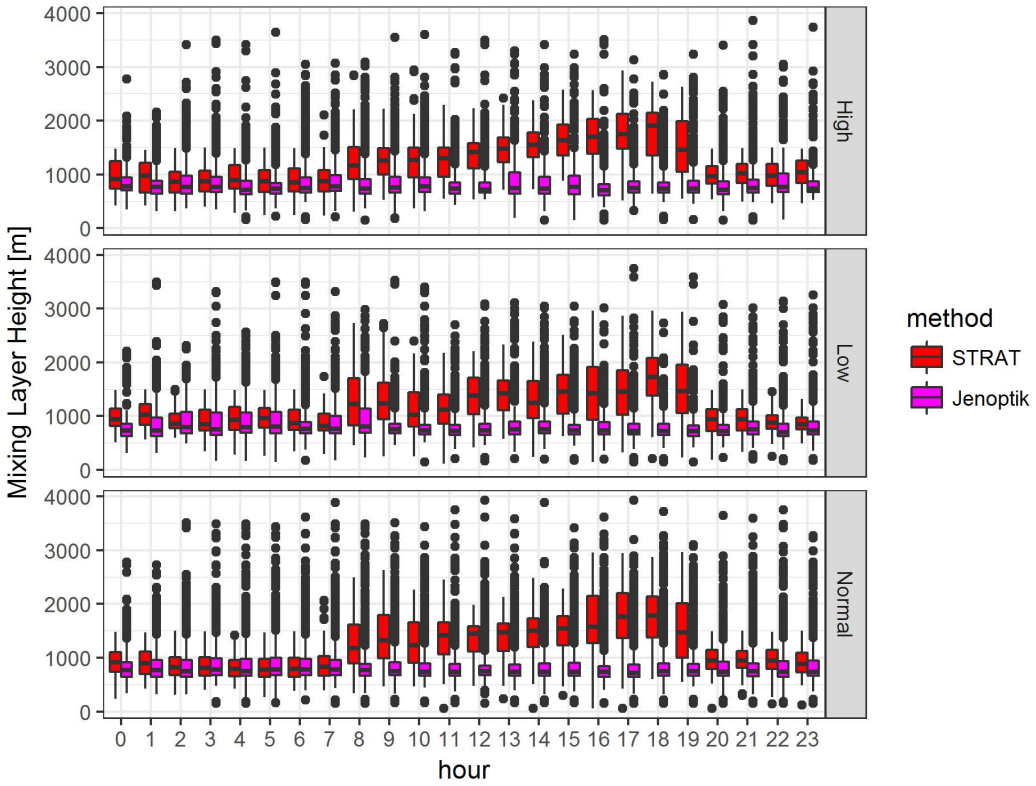

Figure 5. Diurnal cycle of the MLH over Sofia determined by STRAT (red) and Jenoptik (magenta) algorithms as a box and whiskers plot (in Tukey's style) at "High", "Low" and "Normal" atmospheric pressure in summer of 2015

4. Conclusions

In this paper, three summer months of MLHs derived by different algorithms from radiosonde and ceilometer data were analyzed and compared. It was shown that Richardson and parcel methods give same MLHs indicating that ML is mainly thermally driven. Lapse rate method underestimate MLH than both aforementioned techniques especially at high atmospheric pressure systems. It was also found that threshold values for potential temperature higher than 2K/km or smaller than 1K/km deteriorate the agreement of lapse rate with Richardson and parcel methods. Based on performed comparison, it was shown that ceilometer derived aerosol profiles could provide reliable information for MLH tracing in urban area. It was also found that provided by Jenoptik algorithm has some difficulties due to its real time operation on single profile which does not exploit previously collected data. Contrary, STRAT showed passable agreement with retrieved by Richardson method MLHs. The observed differences between lidar- and radiosonde-based MLH are due in part to the distance between the two instruments locations and partly to the different tracers used in each algorithm. The main problems of lidar-based techniques were identified as layer attribution, especially at night and in transition periods when aerosol layers aloft were misleadingly chosen by algorithms. It was underlined that uncomplete overlapping of ceilometer hampers detection of low MLH at night. Based on the performed statistical analysis it was shown that STRAT algorithm reconstructs expected MLH increase in the morning until afternoon with daily maximum in the late afternoon. On the other hand, the Jenoptic method showed some difficulties with tracking of MLH diurnal evolution and sometimes reported too high values.

Funding: This research and publication costs were funded by the Bulgarian National Science Fund grant number DM 04/1 2016.

Acknowledgments: This study would not be possible without TOPROF – European COST action ES1303 and the advices and recommendations of all TOPROF members. The author is also grateful to NOAA's National Centers

for Environmental Information for providing the IGRA. Acknowledgments are due to all contributors to the R project . The author would also like to thank anonymous referees whose valuable comments and corrections significantly improved paper quality.

Conflicts of Interest: The author declare no conflict of interest.

References

1. Seibert, P.; Beyrich, F.; Gryning, S.E.; Joffre, S.; Rasmussen, A.; Tercier, P. Review and intercomparison of operational methods for the determination of the mixing height. *Atmospheric environment* **2000**, *34*, 1001–1027. doi:10.1016/S1352-2310(99)00349-0.
2. Schäfer, K.; Emeis, S.; Hoffmann, H.; Jahn, C. Influence of mixing layer height upon air pollution in urban and sub-urban areas. *Meteorologische Zeitschrift* **2006**, *15*, 647–658. doi:10.1127/0941-2948/2006/0164.
3. Schäfer, K.; Wagner, P.; Emeis, S.; Jahn, C.; Muenkel, C.; Suppan, P. Mixing layer height and air pollution levels in urban area. Remote Sensing of Clouds and the Atmosphere XVII; and Lidar Technologies, Techniques, and Measurements for Atmospheric Remote Sensing VIII. International Society for Optics and Photonics, 2012, Vol. 8534, p. 853409. doi:10.1117/12.974328.
4. Yuan, J.; Bu, L.; Huang, X.; Gao, H.; Sa, R. Particulate Characteristics during a Haze Episode Based on Two Ceilometers with Different Wavelengths. *Atmosphere* **2016**, *7*, 20. doi:10.3390/atmos7020020.
5. Zang, Z.; Wang, W.; Cheng, X.; Yang, B.; Pan, X.; You, W. Effects of Boundary Layer Height on the Model of Ground-Level PM2. 5 Concentrations from AOD: Comparison of Stable and Convective Boundary Layer Heights from Different Methods. *Atmosphere* **2017**, *8*, 104. doi:10.3390/atmos8060104.
6. Geiß, A.; Wiegner, M.; Bonn, B.; Schäfer, K.; Forkel, R.; Schneidemesser, E.v.; Münkel, C.; Chan, K.L.; Nothard, R. Mixing layer height as an indicator for urban air quality? *Atmospheric Measurement Techniques* **2017**, *10*, 2969–2988. doi:10.5194/amt-10-2969-2017.
7. Mues, A.; Rupakheti, M.; Münkel, C.; Lauer, A.; Bozem, H.; Hoor, P.; Butler, T.; Lawrence, M.G. Investigation of the mixing layer height derived from ceilometer measurements in the Kathmandu Valley and implications for local air quality. *Atmospheric Chemistry and Physics* **2017**, *17*, 8157–8176. doi:10.5194/acp-17-8157-2017.
8. Zeng, S.; Zhang, Y. The Effect of Meteorological Elements on Continuing Heavy Air Pollution: A Case Study in the Chengdu Area during the 2014 Spring Festival. *Atmosphere* **2017**, *8*, 71. doi:10.3390/atmos8040071.
9. Kotthaus, S.; Halios, C.H.; Barlow, J.F.; Grimmond, C. Volume for pollution dispersion: London's atmospheric boundary layer during ClearfLo observed with two ground-based lidar types. *Atmospheric Environment* **2018**, *190*, 401 – 414. doi:https://doi.org/10.1016/j.atmosenv.2018.06.042.
10. Baklanov, A. The mixing height in urban areas–a review. *Mixing heights and inversions in urban areas, COST Action* **2002**, *715*, 9–28.
11. Schäfer, K.; Emeis, S.; Jahn, C.; Münkel, C.; Schrader, S.; Höß, M. New results from continuous mixing layer height monitoring in urban atmosphere. Remote Sensing of Clouds and the Atmosphere XIII. International Society for Optics and Photonics, 2008, Vol. 7107, p. 71070A. doi:10.1117/12.800358.
12. Vishnu, R.; Kumar, Y.B.; Sinha, P.R.; Rao, T.N.; Samuel, E.J.J.; Kumar, P. Comparison of mixing layer heights determined using LiDAR, radiosonde, and numerical weather prediction model at a rural site in southern India. *International Journal of Remote Sensing* **2017**, *38*, 6366–6385. doi:10.1080/01431161.2017.1354264.
13. Schween, J.; Hirsikko, A.; Löhnert, U.; Crewell, S. Mixing-layer height retrieval with ceilometer and Doppler lidar: from case studies to long-term assessment. *Atmospheric Measurement Techniques* **2014**, *7*, 3685–3704. doi:10.5194/amt-7-3685-2014.
14. Lokoshchenko, M.A. Long-term sodar observations in Moscow and a new approach to potential mixing determination by radiosonde data. *Journal of Atmospheric and oceanic Technology* **2002**, *19*, 1151–1162. doi:10.1175/1520-0426(2002)019<1151:LTSOIM>2.0.CO;2.
15. Emeis, S.; Türk, M. Frequency distributions of the mixing height over an urban area from SODAR data. *Meteorologische Zeitschrift* **2004**, *13*, 361–367. doi:10.1127/0941-2948/2004/0013-0361.
16. Stull, R.B. *An introduction to boundary layer meteorology*; Vol. 13, Springer Science & Business Media, 2012. doi:10.1007/978-94-009-3027-8.
17. Sicard, M.; Perez, C.; Comeren, A.; Baldasano, J.M.; Rocadenbosch, F. Determination of the mixing layer height from regular lidar measurements in the Barcelona area. Remote Sensing of Clouds and

the Atmosphere VIII. International Society for Optics and Photonics, 2004, Vol. 5235, pp. 505–517. doi:10.1117/12.511481.

18. Cimini, D.; De Angelis, F.; Dupont, J.C.; Pal, S.; Haeffelin, M. Mixing layer height retrievals by multichannel microwave radiometer observations. *Atmospheric Measurement Techniques* **2012**, *6*, 2941–2951. doi:10.5194/amt-6-2941-2013.
19. Holzworth, G.C. Estimates of mean maximum mixing depths in the contiguous United States. *Mon. Weather Rev* **1964**, *92*, 235–242. doi:10.1175/1520-0493(1964)092\%3C0235:EOMMMD\%3E2.3.CO;2.
20. Wang, X.; Wang, K. Estimation of atmospheric mixing layer height from radiosonde data. *Atmospheric Measurement Techniques* **2014**, *7*, 1701–1709. doi:10.5194/amt-7-1701-2014.
21. Hennemuth, B.; Lammert, A. Determination of the atmospheric boundary layer height from radiosonde and lidar backscatter. *Boundary-Layer Meteorology* **2006**, *120*, 181–200. doi:10.1007/s10546-005-9035-3.
22. Wiegner, M.; Emeis, S.; Freudenthaler, V.; Heese, B.; Junkermann, W.; Münkel, C.; Schäfer, K.; Seefeldner, M.; Vogt, S. Mixing layer height over Munich, Germany: Variability and comparisons of different methodologies. *Journal of Geophysical Research: Atmospheres* **2006**, *111*. doi:10.1029/2005JD006593.
23. Emeis, S.; Schäfer, K.; Münkel, C. Surface-based remote sensing of the mixing-layer height–a review. *Meteorologische Zeitschrift* **2008**, *17*, 621–630. doi:10.1127/0941-2948/2008/0312.
24. Beyrich, F.; Görsdorf, U. Composing the diurnal cycle of mixing height from simultaneous sodar and wind profiler measurements. *Boundary-Layer Meteorology* **1995**, *76*, 387–394. doi:10.1007/BF00709240.
25. García-Franco, J.; Stremme, W.; Bezanilla, A.; Ruiz-Angulo, A.; Grutter, M. Variability of the Mixed-Layer Height Over Mexico City. *Boundary-Layer Meteorology* **2018**, *167*, 493–507. doi:10.1007/s10546-018-0334-x.
26. Knepp, T.N.; Szykman, J.J.; Long, R.; Duvall, R.M.; Krug, J.; Beaver, M.; Cavender, K.; Kronmiller, K.; Wheeler, M.; Delgado, R.; others. Assessment of mixed-layer height estimation from single-wavelength ceilometer profiles. *Atmospheric measurement techniques* **2017**, *10*, 3963. doi:10.5194/amt-10-3963-2017.
27. Peng, J.; Grimmond, C.S.B.; Fu, X.; Chang, Y.; Zhang, G.; Guo, J.; Tang, C.; Gao, J.; Xu, X.; Tan, J. Ceilometer-Based Analysis of Shanghai's Boundary Layer Height (under Rain-and Fog-Free Conditions). *Journal of Atmospheric and Oceanic Technology* **2017**, *34*, 749–764. doi:10.1175/JTECH-D-16-0132.1.
28. Nemuc, A.; Nicolae, D.; Talianu, C.; Carstea, E.; Radu, C. Dynamic of the lower troposphere from multiwavelength LIDAR measurements. *Romanian Reports in Physics* **2009**, *61*, 313–323.
29. Ungureanu, I.; Stefan, S.; Nicolae, D. Investigation of the cloud cover and planetary boundary layer (PBL) characteristics using ceilometer CL-31. *Romanian Reports in Physics* **2010**, *62*, 396–404.
30. Wang, W.; Gong, W.; Mao, F.; Pan, Z. An improved iterative fitting method to estimate nocturnal residual layer height. *Atmosphere* **2016**, *7*, 106. doi:10.3390/atmos7080106.
31. Li, H.; Yang, Y.; Hu, X.M.; Huang, Z.; Wang, G.; Zhang, B. Application of Convective Condensation Level Limiter in Convective Boundary Layer Height Retrieval Based on Lidar Data. *Atmosphere* **2017**, *8*, 79. doi:10.3390/atmos8040079.
32. Caicedo, V.; Rappenglück, B.; Lefer, B.; Morris, G.; Toledo, D.; Delgado, R. Comparison of aerosol lidar retrieval methods for boundary layer height detection using ceilometer aerosol backscatter data. *Atmospheric Measurement Techniques* **2017**, *10*, 1609–1622. doi:10.5194/amt-10-1609-2017.
33. Haeffelin, M.; Angelini, F.; Morille, Y.; Martucci, G.; Frey, S.; Gobbi, G.; Lolli, S.; O'dowd, C.; Sauvage, L.; Xueref-Rémy, I.; others. Evaluation of mixing-height retrievals from automatic profiling lidars and ceilometers in view of future integrated networks in Europe. *Boundary-Layer Meteorology* **2012**, *143*, 49–75. doi:10.1007/s10546-011-9643-z.
34. Münkel, C.; Eresmaa, N.; Räsänen, J.; Karppinen, A. Retrieval of mixing height and dust concentration with lidar ceilometer. *Boundary-layer meteorology* **2007**, *124*, 117–128. doi:10.1007/s10546-006-9103-3.
35. Uzan, L.; Egert, S.; Alpert, P. Ceilometer evaluation of the eastern Mediterranean summer boundary layer height – first study of two Israeli sites. *Atmospheric Measurement Techniques* **2016**, *9*, 4387–4398. doi:10.5194/amt-9-4387-2016.
36. Stachlewska, I.; Piądłowski, M.; Migacz, S.; Szkop, A.; Zielińska, A.; Swaczyna, P. Ceilometer observations of the boundary layer over Warsaw, Poland. *Acta Geophysica* **2012**, *60*, 1386–1412. doi:10.2478/s11600-012-0054-4.
37. Morille, Y.; Haeffelin, M.; Drobinski, P.; Pelon, J. STRAT: An automated algorithm to retrieve the vertical structure of the atmosphere from single-channel lidar data. *Journal of Atmospheric and Oceanic Technology* **2007**, *24*, 761–775. doi:10.1175/JTECH2008.1.

38. Poltera, Y.; Martucci, G.; Collaud Coen, M.; Hervo, M.; Emmenegger, L.; Henne, S.; Brunner, D.; Haefele, A. PathfinderTURB: an automatic boundary layer algorithm. Development, validation and application to study the impact on in-situ measurements at the Jungfraujoch. *Atmospheric Chemistry and Physics Discussions* **2017**. doi:10.5194/acp-17-10051-2017.
39. Kotthaus, S.; Grimmond, C.S.B. Atmospheric boundary-layer characteristics from ceilometer measurements. Part 1: A new method to track mixed layer height and classify clouds. *Quarterly Journal of the Royal Meteorological Society*, *144*, 1525–1538. doi:10.1002/qj.3299.
40. Griffiths, A.; Parkes, S.; Chambers, S.; McCabe, M.; Williams, A. Improved mixing height monitoring through a combination of lidar and radon measurements. *Atmospheric Measurement Techniques* **2013**, *6*, 207–218. doi:10.5194/amt-6-207-2013.
41. Galeriu, D.; Melintescu, A.; Stochioiu, A.; Nicolae, D.; Balin, I. Radon, as a tracer for mixing height dynamics-an overview and RADO perspectives. *Romanian Reports in Physics* **2011**, *63*, 115–127.
42. Heese, B.; Flentje, H.; Althausen, D.; Ansmann, A.; Frey, S. Ceilometer lidar comparison: backscatter coefficient retrieval and signal-to-noise ratio determination. *Atmospheric Measurement Techniques* **2010**, *3*, 1763–1770. doi:10.5194/amt-3-1763-2010.
43. Jenoptik. *Cloud Height Meter CHM 15k - User Manual*, 2009.
44. Durre, I.; Vose, R.S.; Wuertz, D.B. Overview of the integrated global radiosonde archive. *Journal of Climate* **2006**, *19*, 53–68. doi:10.1175/JCLI3594.1.
45. De Haij, M.; Wauben, W.; Baltink, H.K. *Continuous mixing layer height determination using the LD-40 ceilometer: a feasibility study*; Royal Netherlands Meteorological Institute (KNMI), 2007.
46. Vogelezang, D.; Holtslag, A. Evaluation and model impacts of alternative boundary-layer height formulations. *Boundary-Layer Meteorology* **1996**, *81*, 245–269. doi:10.1007/BF02430331.
47. Menut, L.; Flamant, C.; Pelon, J.; Flamant, P.H. Urban boundary-layer height determination from lidar measurements over the Paris area. *Applied Optics* **1999**, *38*, 945–954. doi:10.1364/AO.38.000945.
48. Sicard, M.; Pérez, C.; Rocadenbosch, F.; Baldasano, J.; García-Vizcaino, D. Mixed-layer depth determination in the Barcelona coastal area from regular lidar measurements: methods, results and limitations. *Boundary-Layer Meteorology* **2006**, *119*, 135–157. doi:10.1007/s10546-005-9005-9.
49. Holzworth, G.C. Mixing depths, wind speeds and air pollution potential for selected locations in the United States. *Journal of applied Meteorology* **1967**, *6*, 1039–1044. doi:10.1175/1520-0450(1967)006\%3C1039:MDWSAA\%3E2.0.CO;2.
50. Garrett, A. Comparison of Observed Mixed-Layer Depths to Model Estimates Using Observed Temperatures and Winds, and MOS Forecasts. *Journal of applied Meteorology* **1981**, *20*, 1277–1283. doi:10.2307/26180297.
51. Dang, R.; Li, H.; Liu, Z.; Yang, Y. Statistical analysis of relationship between daytime Lidar-derived planetary boundary layer height and relevant atmospheric variables in the semiarid region in Northwest China. *Advances in Meteorology* **2016**, *2016*. doi:10.1155/2016/5375918.
52. Lotteraner, C.; Piringer, M. Mixing-height time series from operational ceilometer aerosol-layer heights. *Boundary-layer meteorology* **2016**, *161*, 265–287. doi:10.1007/s10546-016-0169-2.
53. Bruine, M.d.; Apituley, A.; Donovan, D.P.; Klein Baltink, H.; Haij, M.J.d. Pathfinder: applying graph theory to consistent tracking of daytime mixed layer height with backscatter lidar. *Atmospheric Measurement Techniques* **2017**, *10*, 1893–1909. doi:10.5194/amt-10-1893-2017.